HHS Public Access

Author manuscript

Ultrasound Med Biol. Author manuscript; available in PMC 2023 September 01.

Published in final edited form as:

Ultrasound Med Biol. 2022 September ; 48(9): 1762–1777. doi:10.1016/j.ultrasmedbio.2022.05.002.

Development of Tough Hydrogel Phantoms to Mimic Fibrous Tissue for Focused Ultrasound Therapies

Yashwanth Nanda Kumar[1], **Zorawar Singh**[2], **Yak-Nam Wang**[1], **George R. Schade**[2], **Wayne Kreider**[1], **Matthew Bruce**[1], **Eli Vlaisavljevich**[3], **Tatiana D. Khokhlova**[1,4], **Adam D. Maxwell**[1,2]

[1]Center for Industrial and Medical Ultrasound, Applied Physics Laboratory, University of Washington

[2]Department of Urology, University of Washington School of Medicine

[3]Department of Biomedical Engineering and Mechanics, Virginia Polytechnic Institute and State University

[4]Department of Gastroenterology, University of Washington School of Medicine

Abstract

Tissue-mimicking gels provide a cost-effective medium to optimize histotripsy treatment parameters with immediate feedback. Agarose and polyacrylamide gels are often used to evaluate treatment outcomes as they mimic the acoustic properties and stiffnesses of a variety of soft tissues, but they do not exhibit high toughness, a characteristic of fibrous connective tissue. To mimic pathologic fibrous tissue found in benign prostate hyperplasia (BPH) and other diseases that are potentially treatable with histotripsy, an optically transparent hydrogel with high toughness was developed that is a hybrid of polyacrylamide and alginate. The stiffnesses was established using shear wave elastography (SWE) and indentometry techniques and were found to be representative of human BPH ex-vivo prostate tissue. Different phantom compositions and excised *ex-vivo* BPH tissue samples were treated with a 700 kHz histotripsy transducer at different pulse repetition frequencies (PRF). Post treatment, the hybrid gels and the tissue samples showed differential reduction in stiffness as measured by SWE. On B-Mode ultrasound, partially treated areas were present as hyperechoic zones and fully liquified areas as hypoechoic zones. Phase-contrast microscopy of the gel samples showed liquefaction in regions consistent with the target lesion dimensions and correlated to findings identified in tissue sample via histology. The required dose to achieve liquefaction in the hybrid gel was similar to what has been observed in ex-vivo tissue and greater than agarose of comparable or higher Young's Modulus by a factor >10. These results indicate that the developed hydrogels closely mimic elasticities found in BPH

Corresponding author: Yashwanth Nanda Kumar, Center for Industrial and Medical Ultrasound, Applied Physics Laboratory, University of Washington, 1013 NE 40th Street, Seattle WA 98105, Mobile: 480-265-6891, Work: 206-543-3144, ynandaku@uw.edu.

Author Disclosure statement

No disclosures to make with respect to this work.

prostate ex-vivo tissue and have a similar response to histotripsy treatment, thus making them a useful cost-effective alternative for developing and evaluating different treatment protocols.

Keywords

Cavitation; Histotripsy; High-Intensity Focused Ultrasound; Benign Prostatic Hyperplasia; Hybrid Hydrogels; Fibrosis; Tissue Mimicking Phantoms

INTRODUCTION

Tissue mimicking phantoms are an important tool for the development, optimization, and performance testing of therapeutic ultrasound techniques (Kharine et al. 2003; Pogue and Patterson 2006). These phantoms provide a cost-effective medium for direct feedback on optimal treatment strategies in a low-risk environment before continuing to pre-clinical in-vivo models and clinical trials. Tissue phantoms have been characterized and utilized in approximating both soft (*e.g.,* blood and liver) and hard (*e.g.,* whole bone and dental) tissue for therapeutic ultrasound (Culjat et al. 2010). Soft-tissue phantoms include agarose, gelatin, polyacrylamide, polyurethane and oil-based gels with hard tissue phantoms being epoxy or acrylic plastic, among others (Bush and Hill 1983; Cabrelli et al. 2017; Clarke et al. 1994; Kondo et al. 2005; Madsen et al. 1998; Tatarinov et al. 1999; Zell et al. 2007). Certain nuanced phantoms made of polyvinyl alcohol, polyacrylamide or acrylic base and embedded with thermal markers like bovine serum albumin (BSA)(McDonald et al. 2004), red blood cells (RBC)(Maxwell et al. 2011b), thermochromic additives(inks, powders or liquid crystals)(Ambrogio et al. 2020; Ambrogio et al. 2022; Eranki et al. 2019) have also been developed. In some cases, they offer reversibility of thermal HIFU effects for reuse, thus fast tracking the testing process (Morchi et al. 2021).

Though there is a broad variety of phantoms available for mimicking tissues with different stiffnesses suitable for evaluating HIFU ultrasound therapies, for e.g., agarose based phantoms (Vlaisavljevich et al. 2015), there are few material substitutes which adequately represent fibrous tissue with high inherent toughness, a quality that may be especially important in mechanical cavitation-based ultrasound therapies. A typical stress-strain curve for a fibrous tissue is nonlinear with large deformations at lower loads, following which the material becomes stiffer at increasing loads and becomes linear at higher loads (Hori and Lewis 1982). Fibrous tissue in general are very compliant and undergo large strains with load thus leading to an overall larger area under the stress-strain curve and greater total energy input to produce mechanical failure (Hori and Lewis 1982). Some hybrid gel phantoms like Polyacrylamide-alginate also possess a larger area under the stress strain curve (Sun et al. 2012) and this attribute is referred to as inherent toughness or fracture toughness of the material.

Inherent toughness is found in many pathologic tissues, including benign prostatic hyperplasia (BPH), wherein the tissue can form fibromuscular (collagenous) components that toughen the tissue and play a role in producing BPH symptoms (Rodriguez-Nieves and Macoska 2013). Ultrasound techniques have been developed to treat BPH, such as histotripsy, which is a non-invasive therapy that uses short, high-pressure ultrasound

pulses to mechanically fractionate tissue(Roberts et al. 2006). Investigators found early success in treating *in-vivo* canine prostates using high pulse repetition frequencies (PRF), demonstrating histotripsy as a promising treatment modality for BPH (Hall et al. 2009; Hempel et al. 2011; Roberts et al. 2014a; Schade et al. 2012). However, during a subsequent clinical trial, histotripsy did not produce objective improvements in clinical symptoms or changes in prostatic volume (Schuster et al. 2018). A potential reason for the reduced efficacy is due to the differences in mechanical characteristics between non-BPH canine (as tested in the prior pre-clinical models) and human BPH tissue (Zhang et al. 2021). In contrast to non-BPH canine prostate, tough fibromuscular stromal hyperplasia tends to predominate in human BPH making it more resistant to the effects of histotripsy (Shapiro et al. 1992). This reasoning is further supported by multiple prior studies which have shown that fibrous tissues are, in general, more resistant to histotripsy-induced tissue damage (Shapiro et al. 1992)(Mancia et al. 2017; Mancia et al. 2019; Vlaisavljevich et al. 2014; Wang et al. 2018). These biological differences highlight the importance of having preclinical models (*i.e.,* tissue phantoms + animal model) that adequately represent the target tissue.

The heterogeneous nature of prostatic tissue provides a unique challenge in creating an appropriate tissue phantom. Despite being considered a soft tissue, fibromuscular stromal hyperplasia (collagen remodeling) wherein fibrosis leads to an increase in elastic modulus due to collagen and elastin cross-linking (Wells 2013) leave the prostate resistant to the treatment effects of histotripsy (Ishigooka et al. 1996). Traditionally, soft agarose, alginate and polyacrylamide gels have been used as tissue mimics for prostate. Although agarose gels can represent soft glandular elements of prostatic tissue (Yang et al. 2017); they have low toughness and tend to break down easily at low stresses, and existing literature suggests that the fracture toughness for polyacrylamide and alginate gels are small and do not capture the mechanical characteristics of average and tough BPH tissue. Additionally, the phantom must be optically transparent to visualize histotripsy cavitation on high-speed photography. Thus, an ideal phantom would be one that:

1. Can approximate the mechanical and acoustic properties of fibrous tissues.
2. Is optically transparent.
3. Can be easily reformulated to approximate a range of tissue properties (*e.g.,* soft, average, and tough BPH tissue with stiffnesses ranging from 15–100 kPa).
4. Responds to histotripsy in a similar manner to tissue in terms of the fracture mechanics and the nucleation and evolution of bubble clouds that cause the mechanical damage.
5. Allows histotripsy lesions to be easily detected (to measure lesion volume and size) and analyzed (in ability to cause complete ablation) for optimization of treatment parameters.
6. Is relatively simple and inexpensive to prepare (Maxwell et al. 2010a).

Such a phantom would be valuable not only for investigation of BPH, but also for other inherently tough, treatment resistant, diseased tissues, including uterine fibroids, fibrous

tumors such as cholangiocarcinoma and pancreatic ductal adenocarcinoma, and plaques caused by Peyronie's disease or atherosclerosis (Hendricks-Wenger et al. 2021; Moreland and Nehra 2002; Schuppan and Afdhal 2008; Stewart et al. 2016). Like BPH, advancements in therapeutic ultrasound for these diseases will depend on identifying effective treatment strategies in accurate preclinical models.

Hydrogels are often used as scaffolds for tissue engineering and to model extracellular matrices for biological studies(Discher et al. 2009). However, traditional hydrogels are limited by their poor mechanical properties and, as a result, double network hydrogel phantoms (with both covalent and ionic crosslinking) were created which have suitable elastic moduli and high mechanical strength (Gong et al. 2003).

In this paper, we fabricate and characterize the mechanical and acoustic properties of a novel three-dimensional polyacrylamide/alginate phantom hydrogel that can better represent tough fibrous tissue such as that found in patients with BPH. The phantoms were compared against ex-vivo human prostate tissue from BPH patients to determine their similarity in response to histotripsy. To evaluate treatment efficacy, B-mode ultrasound was employed along with shear wave elastography (SWE), and changes in cavitation bubble dynamics as seen under high-speed camera photography. In addition, a method utilizing phase contrast microscopy was introduced to visualize damage to the phantom structure. This work establishes the feasibility of using these phantoms to evaluate the efficacy of treatment parameters in ablating ex-vivo fibrous tissue.

MATERIALS AND METHODS

Polyacrylamide Alginate Gel Preparation

A modified polyacrylamide alginate hybrid gel formulation based on prior work reported by (Sun et al. 2012) was developed to mimic pathologic tough fibrous tissues. Several gel ratios (polyacrylamide: alginate) were explored and 3 weight ratios (85:15,90:10,95:5 w/w) were chosen to represent different tissue stiffness (15–100 kPa) and toughness(Sun et al. 2012). The overall volume of the water in the gel was held constant at 86% by weight across all gel samples. Liquid acrylamide (40% solution by weight) was used for preparing the phantom. The photoinitiator ammonium persulphate (APS), the covalent crosslinker N,N-methylenebisacrylamide (MBAA) and the crosslinking accelerator N,N,N',N'-tetramethylethylenediamine (TEMED) were kept at ratios of 0.0017, 0.0006, 0.0028 respectively to the weight of acrylamide. As an additional step, 10 mL of 1% by weight of MBAA and APS were prepared to safely titrate the components into the mixing beaker, due to the minute quantities required for weighing and the resolution of the balance. The weights of these 3 components were in addition to the sum total. The recipe is summarized in Table I. For the other gel ratios, the alginate weight was increased, and the ratio of acrylamide reduced accordingly, and the quantity of the other components adjusted. All required chemical ingredients were sourced from Sigma Aldrich Inc (St. Louis, Montana, USA).

In a fume hood, the preparation was started by adding the required volume of deionized water into a beaker. Sodium alginate was weighed using a weigh scale (PB153-S, Mettler

Toledo, Columbus, Ohio, USA) and transferred into the beaker which was then placed on a magnetic stirrer and mixed at an RPM of 300 until the alginate was completely dissolved to form a homogeneous solution. During this process, an ultrasonic processor (Vibra-Cell - VCX 500, Sonics & Materials Inc., Newtown, Connecticut, USA) was used at 25% amplitude to sonicate the sample for ~60 seconds to assist with the dissolution process for every 2–3 minutes of stirring. The required volume of acrylamide was then measured using a graduated beaker and poured into the alginate solution and stirred. The beaker was then covered with perforated aluminum foil and placed in a degassing chamber for an hour at 25 inHg vacuum. Alongside this, prepared 1% (by weight) solutions of MBAA and APS were also degassed along with an additional 500–1000 mL of deionized water. After degassing, the contents of AP, MBAA and TEMED were pipetted to the beaker and mixed using a magnetic stirrer at a low RPM of 60. The contents were transferred into multiple molding beakers to set the thickness of each gel to 2 cm and a diameter of 3 cm.

The gel was cured by UV light in a curing chamber (Form curing oven, Formlabs, Somerville Massachusetts, USA) at 60°C for 3 hours. Post cure, the gel samples were removed from the molding beakers and thoroughly rinsed under running water to remove any residual chemicals. Further curing was performed by submerging the UV-cured gel in a crosslinking solution. Calcium sulfate dihydrate $CaSO_4.2H_2O$, the ionic crosslinker for the alginate, was prepared by mixing the powder into degassed and deionized water. A 1M solution was chosen to ensure enough calcium ions were present for complete diffusion with extended soaking times to enable complete crosslinking based on the work by (Yang et al. 2013).

The concentration proposed can be used for curing all the gel compositions, as it contains an excess of calcium ions. The gel phantoms were suspended in the solution for a period of 48 hours preferably in a desiccator held at 25 in Hg vacuum or in a sealed container. The time was calculated based on the formula from (Yang et al. 2013)

$$t = \left(\frac{4}{\pi}\right) \cdot \frac{H^2}{D} \qquad \text{Eqn.1}$$

where H is the half thickness of the gel in cm, D = 10^−5 cm^2 s^−1 is the diffusion coefficient. Equation 1 determined the minimum time for submersion to be around 11.3 hours, however the samples were submerged for 48 hours to ensure complete diffusion. After 48 hours, the optically transparent gels were removed from the beaker, rinsed, and stored in an airtight container. Over the recorded storage period of 11 days, the maximum change in weight was found to be <7%. Storage of the gels in water is not recommended, as submergence led to swelling secondary to absorption. The summarized flowchart outlining the steps to pour the gel is shown in Figure 1.

Two additional points are worth noting regarding the gel formulation. First, initial preparations mixed the ionic crosslinker calcium sulfate dihydrate directly into the liquid gel solution prior to UV cure, but this should be avoided as it led to a very heterogeneous gel phantom whose stiffness varied widely across the sample and made it opaque. Second, calcium chloride cannot be substituted as a crosslinker despite its high solubility and fast

cross linking (Ibrahim et al. 2019) (Yang et al. 2013). It's use led to a stiff outer layer with the interior of the phantom at a lower stiffness, and also made the phantom opaque.

Agarose Gel Preparation

Agarose gel was prepared as a 1.5% weight/volume combination of agarose and deionized water by mixing 3 g of agarose to 225 mL of water in a beaker and heated to a boiling temperature for 6 minutes. This yields a final volume equal to 200mL which constitutes the 1.5% weight/volume gel. The gel was slowly cooled by placing it in a desiccator kept at 25 inHg to prevent any dissolution of air back into the gel, and once the mixture reached a temperature below 45°C, the contents were transferred into an acrylic container measuring 5cm × 5cm × 8cm. When agarose was used to embed hybrid gel phantoms and tissue, the same process was followed with the addition of submerging the target within agarose during the cooling process.

Measurement of Physical and Acoustical Properties

The weights of the gels were measured using a standard analytical laboratory balance and the volume using a water displacement technique in a beaker, thus yielding the density measurements. The frequency dependent attenuation and the speed of sound were measured using a through-transmission water substitution method as described in (Dunmire et al. 2013). Two ranges of frequency 500–800 kHz and 2.0–2.3MHz were utilized in the measurement process. A linear fit regression line with zero intercept was used to calculate the slope in dB/MHz. The slope was divided by the measured thickness of the gel to yield the attenuation coefficient in dB/cm/MHz.

To determine whether these samples could be used at elevated temperatures (such as boiling histotripsy), separate gel samples were vacuum sealed in food saver bags and submerged in a temperature-controlled water bath using an immersion circulator (Model No. 1112A, VWR, Randor, USA). The bath was maintained at 98°C, and the gels were kept in place for an extended period to observe if the gels remained in a solid state or melted. After the submergence period, the gels were removed from the bags, blotted, and weighed to determine if there was any significant weight loss.

Two techniques were used to estimate the stiffness (Young's modulus) of the gels, one using shear wave elastography (SWE) with an Aixplorer ultrasound platform (Supersonic Imagine, Aix-en-Provence, France) and the other using a custom-made spherical indenter setup (indentometer).

For SWE, an SL15–4, a 256-element linear transducer (Supersonic Imagine, Aix-en-Provence, France) with a bandwidth of 4–15MHz was mounted on to a custom built manual linear positioning system, as illustrated in Figure 2. A set of 16-gauge copper wires were embedded into the hybrid gels to act as locational references. The pins were positioned so that each remained several cm from the actual measurement zone. The gel was then placed in a container of deionized water lined with rubber to absorb and reduce reverberations. Measurement zones were identified and marked at known distances away from the reference pins. Each frame captured provided a 2D image with shear wave data, and regions of interest were identified. The medium is assumed incompressible; therefore the shear modulus is

multiplied by a factor of 3 by the system to obtain the Young's modulus taking into account normal density of tissue. The size of each region of analysis ranged from 2–5mm in diameter and the data was recorded for each slice. A 3-dimensional SWE stiffness map with the Young's modulus was recorded by moving the positioning system in intervals of 1mm and collectively stacking the data across all frames. The transducer setup was operated in phantom penetration mode to get the most complete B-mode image and SWE based stiffness data which were subsequently recorded.

A custom indentometer was built using a spherical ball indenter (8 mm diameter) attached to a vertical linear positioning stage consisting of a linear slide drive driven by a lead screw and connected to a stepper motor. The 8mm ball diameter was chosen with relative to the size of the gels made which were ~20mm in thickness, to keep the contact radius and the displacement small compared with the sample size (Choi and Shield 1981). An Arduino Uno microcontroller board (Arduino, Somerville, MA) with a motor driver shield was used to control the displacement of the indenter via MATLAB (MathWorks., Inc, Natick, MA). The force corresponding to each displacement was measured by a laboratory balance (Acculab ALC-320-3; Sartorius Mechatronics Corp., Bohemia, NY, USA) as the change in effective weight of the gel sample. These components allowed programmatic control of displacement with a resolution of 2.5 μm along with force measurements with a resolution of 1 mg. A few drops of water were placed onto the sample. The weigh scale was tared and the indenter was brought into contact with the water droplet. The surface tension of the water pulling away from the gel surface on the hemisphere resulted in a net negative weight displayed on the. As the indenter was bought close to the sample and nearly made contact, the net weight became net zero thus ensuring it was at a null position. The indenter was then lowered in small steps (step size −0.2 mm) with a speed of (1 step/second) while recording the weight measured by the balance vs the indenter displacement. Previous works (Dunmire et al. 2013; Guntur and Choi 2014; Khokhlova et al. 2020), have reported in detail the measurement technique. The shear modulus μ was then calculated from the following equation:

$$F^{\left(\frac{2}{3}\right)} = \left(\frac{16\mu}{3}\right)^{2/3} R^{\frac{1}{3}} \cdot d, \qquad \text{Eqn.2}$$

where F is the force acting on the balance, R is the radius of the indenter, and the d is the sample displacement. The net Poisson's ratio was reported to be close to 0.5 (Szabo 2004) thus, the conversion to Young's modulus was to be done by multiplying the shear modulus by a factor of 3.

The indentometer setup was calibrated using Zerdine pucks with reported Young's modulus acquired from Computerized Imaging Reference Systems, Inc (Norfolk, Virginia, USA).

Experimental Setup and Characterization of Histotripsy Exposures:

An 18-element 700 kHz transducer with an aperture of 13 cm and focal distance of 11 cm was used to mimic the commercial transducer developed by HistoSonics, Inc (Roberts et al. 2014b). The transducer was designed and fabricated with a central cavity to house coaxially a M5Sc ultrasound imaging probe of a GE Vivid E9 4D ultrasound system (GE Healthcare, Chicago, USA). A custom-built class D amplifier powered by a high voltage

source (TDK Lambda GENH6001.3) with an appropriate electrical matching network was used to drive the transducer. The beamwidth of this transducer's acoustic field at −6dB level was measured at low output level, under linear propagation conditions using a lipstick hydrophone (HGL-0085, ONDA Corporation, Sunnyvale, CA) and was 13.25mm axially and 2.3mm laterally. At higher output levels, the peak focal pressures produced by the transducer were recorded using a fiber-optic probe hydrophone (FOPH2000, RP Acoustics, Stuttgart, Germany). The highest output levels used in the experiment corresponded to peak positive pressure of 103 MPa, and peak negative pressure of 20 MPa. Output levels were controlled by actively modifying the input DC voltage applied to the amplifier. After submergence into a tank filled with degassed deionized water, the position of the transducer relative to the gel was controlled using a three-axis motorized positioner with linear slides driven by lead screws and stepper motors (Velmex Bislides and VXM controller, Bloomfield, New York, USA). Agarose gels or hybrid gels (embedded in agarose) were placed into the tank using a fixture with an acoustic window that introduced minimal disruption to the acoustic pressure field. The fixture location was controlled by the motorized positioner.

Treatment Parameters:

Previous work using histotripsy to treat BPH was used as a basis for parameter selection. From the prior work by (Roberts et al. 2014a) utilizing the commercial system, the following pulse parameters were used: the center frequency was set to 700 kHz with a pulse repetition frequency (PRF) of 500 Hz and pulse duration of 3 cycles (hereafter referred to as "high-PRF" settings). The dosage was established from the prior clinical study and estimated to be equivalent to a pulse count of 25000 per point (Schuster et al. 2018). A higher dose of 50000 pulses/point was also explored under the same parameters in a subset of phantoms.

Due to the limited efficacy of the high-PRF parameters in producing objective improvements in the prior clinical trial, a low-PRF (10 Hz) exposure was also tested, based on studies indicating that low-PRF, long pulse duration parameters resulted in more complete ablation due to the formation of larger bubble clouds (Maxwell et al. 2011a; Wang et al. 2012b). The pulse count was determined from the dose response performed in hybrid gels (Table 2). The alternate parameter settings will be referred to, hereafter, as "low-PRF" settings. These treatment parameters were tested in order to establish robust correlation of histotripsy response in hybrid gels to *ex-vivo* BPH tissue. The pressure levels for creating volumetric lesions in gels and prostate, as well as evaluating the dose response of the gel were determined at +10% of the pressure threshold observed by imaging for creating sustained cavitation clouds.

Hydrogel Histotripsy Response Experiments

Four sets of experiments were conducted to determine how the hydrogel phantoms compared with existing tissue phantoms and ex-vivo tissue, as well as their response to histotripsy sonication. These experiments are delineated below. A detailed diagram of the bench top hybrid gel experimental test and visualization (high Speed camera, LED light source, focusing lens and power source) setup is presented in Fig 3. For treating tissues, a similar setup was used without the visualization.

(i) Volumetric Treatment Experiments: The goal of these experiments was to determine the changes in the gel through B-mode imaging, SWE and visual inspection of lesion using phase contrast microscopy when creating volumetric histotripsy lesions. Phase contrast microscopy uses an optical mechanism that translates phase variations in the gel into light intensity changes that can be visualized as differences in contrast. Untreated regions have uniform, intensity, with treated regions having varying contrast. The gels were sectioned and visualized using a Nikon Eclipse 80i; Nikon at 4x magnification using a phase contrast filter. A series of images were taken and stitched through NIS elements (Nikon Instruments Inc, Melville, New York, USA) to visualize the complete set of lesions and qualitatively deduce the dose response. To create volumetric lesions, gels (n=3 per type) were first mounted on a fixture and placed into a tank of degassed and deionized water as shown in Figure 3. Volumetric treatment zones were then created by translating the gel sample with the motorized positioner in a raster fashion with 1.15mm steps within a 3×3 rectangular grid. At each step a certain number of pulses was applied: 25K or 50K per step at the high-PRF setting, and 10k per step at the low-PRF setting. Post treatment, treatment efficacy was evaluated with B-mode US, looking for hypoechoic changes indicating complete liquefaction. (Wang et al. 2011). For SWE, pre-treatment SWE measurements of the hybrid gels (of each formulation) were taken to establish stiffness. Post-treatment the stiffness of the gels was remeasured at the same designated sites from earlier using the SWE setup to evaluate the stiffness reduction, as would be expected from tissue treated with histotripsy (Wang et al. 2011). A Wilcoxon signed rank test was utilized to measure the change in stiffness in each region, before and after treatment. The reason for choosing a Wilcoxon signed rank test was due to presence of right censored data observed with some of the shear wave measurements. The statistical significance was set at $P < 0.05$. The SWE and B-Mode data were analyzed over 3 frames for each sample where visual cues showed a change in B-mode and SWE. The frames were chosen such that the analysis covered a frame at the beginning of lesion, at the middle and towards the end of the lesion, thereby including the edge cases.

(ii) Prostate Tissue Experiments: The purpose of this set of experiments was to compare changes in tissue with those observed in the gel phantoms. Deidentified ex-vivo human BPH prostate tissue samples (n = 3 for each test setting) acquired from simple prostatectomies from patients with symptomatic BPH and were sonicated to produce volumetric liquified regions. The tissue samples ranging from 5–10 cc were embedded in 1.5% agarose gels prepared as described above and the experiments were performed within 6–8 hours of collection. B-mode and SWE measurements were taken at designated locations prior to the treatment to establish baseline stiffness. The embedded sample was placed in a water tank filled with deionized and degassed water. The sample was visualized with coaxial ultrasound imaging probe, and the transducer focus was positioned at 5mm depth within the sample. The pressure levels for prostate tissue experiments were determined at +10% of the threshold observed for creating sustained cavitation clouds in the range included in Table 2. Using a motorized positioner, treatments were performed in a grid (ranging from 3×3 to 6×6 points) spaced in a plane orthogonal to the propagation axis of the transducer at both high-PRF and low-PRF exposures with step size of 1.15 mm so the foci overlapped to create a volumetric lesion. Grid sizes were varied depending on size of respective prostate

samples. A pulse count of 25K and 50K per point was used for the high-PRF exposure, which translated to 14.4 and 28.8 seconds treatment per step. For the low-PRF exposure, a pulse count of 5K and 10K was used, which translated to 144 and 288 seconds per point. Post treatment, the samples were reimaged using B-mode and SWE (data collected from 3 frames) and sections of the sample containing the treated lesion were fixed in formalin for histological analysis (Masson's trichrome & hematoxylin and eosin staining). A Wilcoxon signed rank test was utilized as done prior with the gels to measure the change in stiffness in each region, before and after treatment with the statistical significance set to $P < 0.05$.

(iii) Bubble Activity Experiments: The goal of this experiment was to compare the bubble cloud generated across different gels and treatment parameters based on the techniques described in (Lin et al. 2014b). The following steps outline the methodology for capturing bubble cloud activity. A current controlled source coupled with a LED light was used to illuminate the path of the treatment with the help of a collimating lens. The high-speed camera (Photron Fastrax APS-RX, Photron, San Diego, California, USA) with an 80–200 mm zoom lens and bellows extension was used to capture bubble activity across different treatment paradigms. A delay of 80 μs was maintained between the input pulse sent to the transducer and the camera trigger, to enable the camera to capture the bubble cloud formed 8 μs after the wavefronts arrive at the focus. The shutter speed was set to 2 μs to capture a single frame for every pulse. The amplifier and the motorized setup were controlled via MATLAB using a custom-built program (Wang et al. 2012b). Both the agarose and hybrid gels (all 3 formulations, n=1) were sonicated with both parameter combinations at an acoustic pressure of 20 MPa P-ve, and the bubble cloud generated was captured using the high-speed camera over 2000 frames. Captured bubble cloud data was compared qualitatively to determine differences in bubble size and cloud dynamics (whether bubbles are dissolving between pulses).

(iv) Dose Response Experiments: The purpose for this set of experiment was to evaluate the dose response of the 85/15 hybrid gel to a fixed set of histotripsy parameters in comparison to the standard 1.5% agarose gel (n=1) of comparable stiffness. From this measurement, the lesion development in the gels as a function of pulse count was evaluated at a single acoustic focal site. Pressure amplitudes were set based on the threshold for sustained cavitation clouds and operated at +20% to form a single lesion. Pressure thresholds varied across both gel formulations and exposure settings but were within the range found in Table 2. The focus of the transducer was placed approximately 5mm beneath the surface of the gel. The pulse count was varied from 20–3000 pulses in the agarose gel and from 100–10000 pulses for the (85/15) hybrid gel.

RESULTS

Measurement of Physical and Acoustical Properties

To evaluate polyacrylamide/alginate gels that mimic ex-vivo human prostate tissue, we first established the mechanical properties inherent to prostate tissue. Using SWE, we determined the Young's modulus of ex-vivo human prostate specimens (n=17). As shown in Figure 4, the median Young's modulus of ex-vivo human prostate tissue was 55.4 kPa but varied over

a large range of from 15.1kPa to 124.4 kPa. The gels increased in stiffness as the ratio of alginate was increased. On shear wave elastography, the gels had median Young's moduli of 90.1, 62.7, and 41.3 kPa for 85/15, 90/10 and 95/05 gels, respectively. Figure 4 illustrates that the different gel compositions approximate the Young's moduli of BPH tissue across its stiffness range, although do not necessarily reach the extremes. Table 3 captures the calculated means and percent deviation of the gels and the tissue, and show the gels to be relatively homogeneous with the tissue showing more heterogeneity as expected.

Three hybrid gels from each configuration were measured using both shear wave elastography and indentometry and the results are summarized in Table 4. In general, the indentometer reported lower stiffness values with respect to SWE across all gel compositions by a similar margin. Additionally, the Young's moduli of the measured agarose gels (n=3) yielded a value of 109.2±3.3 kPa, by indentometry.

Table 5 highlights the acoustic properties including density, speed of sound, impedance, and attenuation. The acoustic properties of the hybrid gels were in-line with other well-established hydrogels (agarose) and had values representative of prostate tissue, although the attenuation was somewhat lower and similar to other pure hydrogels. There were small variations in acoustic properties between different gel compositions across various ratios of polyacrylamide to alginate without clear trends. The values ranged from 1020 – 1056 kg/m^3, 1514 – 1528 m/s, 1.54 −1.61 MRayls and 0.06 to 0.14 dB/cm/MHz for density, speed of sound, acoustic impedance, and attenuation, respectively.

Histotripsy Response Experiments

(i) Volumetric Treatment Experiment—We tested the functionality of the hydrogels as tissue phantoms for histotripsy. Two primary measurements for evaluating treatment effects in the hybrid gels were captured: echogenic changes on B-mode ultrasound imaging and Young's modulus changes on SWE. B-mode images in Figure 5a demonstrate hyperechoic changes in all three gel formulations treated with the high-PRF exposures. However, these hyperechoic changes on B-mode did not translate to a marked difference between Pre to Post treatment regions on the SWE color map when treated with the high-PRF histotripsy parameters. In comparison, the low-PRF parameters produced defined lesions in the hybrid gels as demonstrated by B-Mode images in Figure 5B where a hypoechoic center bordered by a hyperechoic rim is observed. These changes noted on B-mode corresponded to marked changes in the Young's moduli of the hypoechoic region as evidenced by the clear changes in the SWE color map for each gel formulation.

Quantitative assessment of the change in Young's moduli (Table 6) further demonstrated the findings seen qualitatively in the SWE color map.

(ii) Prostate Tissue Experiment—To determine the utility of hybrid gels in predicting efficacy of treatment parameters in prostate tissue samples, ex-vivo human prostatic tissue samples were treated with both high-PRF and low-PRF exposures, with figure 6 highlighting the high-PRF-High dose and low-PRF sonication for a 90–10 gel and prostate tissue of similar stiffness. Histotripsy damage was visualized under phase contrast microscopy at different parameter settings within hybrid gels and treatment effects in prostate tissue were

evaluated histologically with H&E and Masson's trichome stains. As shown in Figure 6A, phase contrast imaging of hybrid gels at the high-PRF parameter settings show sparse damage; whereas the low-PRF parameter settings produced higher overlap between lesions and the expected area of treatment. The histologic findings (Figure 6B) were consistent with findings seen in under phase contrast illumination for gels (Figure 6A).

Treatment with high-PRF parameters yield discrete pockets of damage rather than a contiguous homogenized lesions indicating poor concordance between actual and expected treated areas for both the hybrid gel and the prostate tissue, covering only 19% and 12% of the expected area respectively as measured from the phase contrast image and histology section. In contrast, the treatment area generated by the low-PRF parameter settings was higher with damage seen over 72% and 66% of the expected area for the hybrid gel and tissue respectively. However, at low-PRF exposures there were some intact structures (fibromuscular stroma with glandular elements) within the treatment area surrounding otherwise homogenized tissue. Some visible artifacts (darkened spots) were also noted with the high-PRF gel phase contrast images. These were a result of the equipment's optical limitation and the slice thickness of the sample. Quantitative assessment of the change in Young's moduli pre and post treatment for the prostate at all sonications are summarized in Table 6.

The 95/5 hybrid gel exhibited a significant change in elasticity from treatment with $p<0.005$ for all exposures indicating liquefaction. For the prostate, change in Young's modulus was significant with a P value of <0.05 and <0.005 with the high-PRF- High dose (50k pulses/step) and the low-PRF exposures respectively, while no significant difference was seen with the high-PRF – Low Dose (25k pulses/step) exposure. For the 90/10 and 85/15 hybrid gel, the change in Young's modulus was significant with a P value <0.005 with the low-PRF sonication indicating liquefaction, while no significant change was observed for any of the high-PRF low or high dose sonications.

(iii) Bubble Activity Experiment—Cavitation cloud images were recorded by high-speed photography for each exposure in the hybrid and 1.5% agarose gels. Figure 7a highlights the difference in the cavitation cloud between agarose gels and hybrid gels (90/10 for example) over frames 1, 500, 1000, and 2000 while part B shows the overlay of the bubble cloud over 2000 frames. The transducer is placed on the left relative to the frame with the focus towards the center of the frame. The bubble cloud typically forms at the focus and grow towards the transducer. In agarose gels, irrespective of the PRF, the cloud appeared predominantly around the focus, with bubbles appearing at different locations between pulses, although appearing denser with the low-PRF exposure. In the hybrid gels, the cloud pattern appeared static (*i.e.*, bubbles formed in the same locations between pulses) with minimal cloud changes throughout the high-PRF exposure for all 2000 frames. In contrast, when treated with the low-PRF exposure, there was an observable increase in the cloud area and formation of new bubbles in successive pulses. The bubble area increase, as seen in Figure 7b was also substantially greater than the agarose gel exposed to similar exposures. In the agarose gel, the increase in bubble area between the high and low-PRF exposure parameters was about 6% and for the hybrid gel the difference was an average of 83%.

(iv) Dose Response Experiment—Figure 8 shows the dose response to low-PRF exposures under phase contrast microscopy in an 85/15 polyacrylamide hydrogel and a 1.5% agarose gel. Both gels were treated at different doses to determine the minimal threshold to produce a liquefied cavity. As seen in Figure 8, the hydrogels show damage at 400 pulses but appear similar up to 3000 pulses. The damage caused optical variations within the hybrid gels, but failed to form a complete liquefactive cavity, covering only 37% of the total lesion volume. In contrast, histotripsy damage with low-PRF exposures produced prominent damage in 1.5% agarose gels at 200 pulses with complete cavity formation occurring at 300 pulses, indicating more rapid breakdown of the gel. These images show that hybrid gels of similar stiffness are more resistant to histotripsy, as evidenced by the minimal cavity formation even with 10 times the dose administered to agarose gel.

DISCUSSION

The results demonstrate that the developed phantoms produce a response to histotripsy comparable to BPH ex-vivo tissue and is similar in terms of acoustical and mechanical properties, making it an appropriate candidate for optimizing treatment parameters. A variety of gel phantoms were explored in the past for treatment optimization, visualization and feedback by different researchers, including agarose lined with red blood cells (Lin et al. 2014a; Maxwell et al. 2011b), polyurethane (Kondo et al. 2005; Pogue and Patterson 2006), collagen(Yamanaka et al. 2019), agar, gelatin (Dunmire et al. 2013) polyacrylamide(Geoghegan et al. 2019; Guan et al. 2016; Guntur and Choi 2014; Khokhlova et al. 2017a). While these gels closely approximate both the acoustic and mechanical properties of soft tissue, they do not explicitly mimic the toughness of fibrous tissue. The stiffness and toughness of the current hybrid gel described in this paper could be modified by simply manipulating the ratio of acrylamide -alginate with the gels becoming highly stiff and tough as the alginate content increased (Sun et al. 2012; Yang et al. 2013). The results also further indicate that stiffness alone does not determine treatment efficacy, and that toughness is an important factor, as seen in the dose response experiments (Figure 8) where the number of pulses required to treat the agarose was only one-tenth that of the hybrid gel of similar stiffness. The reason for the increased toughness of this phantom is the cross linking of the alginate chains involving an improved ionic cross linking between calcium and carboxyl ions (Sun et al. 2012), which is similar to the collagen and elastin cross linking seen in fibromuscular hyperplasia typical for BPH tissue vs weak hydrogen boding in the agarose. Fibrous tissues in general respond non-linearly to external stress, a characteristic that explains the high fracture toughness of these materials, but such materials have been treated with histotripsy effectively in the past with increased pulse count (Schade et al. 2014) (Maxwell et al. 2014)

The acrylamide-alginate hybrid gel provides multiple avenues to analyze treatment efficacy. The high transparency of the gels enables study the dynamics of cavitation through high-speed camera observations of the bubble cloud. The transparency also allowed immediate post-treatment observation of the lesion dimensions through the use of phase contrast microscopy as explored in this study. It was shown that treated regions are easily identifiable as the damage produces minor variations in the optical homogeneity of the gel, which further assist in analyzing the extent of damage.

The hybrid gels also appear to contain acoustic scatterers, thus providing a way to subject them to ultrasound imaging techniques like B-mode and SWE. B-mode imaging was successfully used in the past with RBC – agarose phantoms (Maxwell et al. 2010b) and BSA – polyacrylamide gels (Choi et al. 2013), where RBCs and BSA act as scatterers. SWE was shown to ascertain viscoelastic properties of the medium (Bercoff et al. 2008) and as a successful imaging feedback technique in treating tissue (Wang et al. 2012a). The hydrogels respond to histotripsy treatment in a way similar to ex-vivo tissue, in that fully treated volumetric lesions resolve with hypoechogenicity on B-mode, with clear changes in the SWE mapping. Partially treated areas often resolved as hyperechoic zones due to potential disruption in the crosslinking, but that did not necessarily show significant change in stiffness. While the possible explanation and mechanism is not well understood at this point, it is possible that as the gel is partially damaged, it creates areas of heterogeneity, with ‘disrupted’ and intact regions with different density, and the size of these regions may have acoustic heterogeneity on a scale that leads to more scattering.

The response of the gels was found to be different between sets of exposure parameters. high-PRF parameters tested across the different experiments showed minimal damage both in tissue and in hybrid gels in most of the cases, whereas low-PRF parameters consistently showed significant damage. The bubble clouds observed in the gels under different parameters showed that they followed the same principles of shock wave scattering as described in previous studies (Maxwell et al. 2011a; Vlaisavljevich et al. 2017). Both in high-PRF and low-PRF exposures in the hybrid gels, once the sonication ended, the bubbles collapse but do not necessarily dissolve immediately, indicating a form of bubble stabilization. They were proportionally longer for the high-PRF settings and with longer dose durations vs the low-PRF exposures. This could possibly be due to the structural differences between the hybrid and the agarose phantom, as such behavior was not observed on the latter. These structural differences could also explain the differences in the observed bubble cloud areas, where in the hybrid gel the bubble cloud comprised smaller bubbles spread over a larger area. In contrast, the cloud comprised larger bubbles confined to a smaller area in the agarose gel. One other possible reason for these observed differences in bubble cloud dynamics could be due to increased bubble nuclei present in hybrid gels which could interact with the incident acoustic field to make the gels more resistant to treatment. In this way, bubble nucleation could be an important distinction between hybrid and agarose gels beyond the differences in structure and potential differences in toughness.

There are several potential reasons for the relatively lower efficacy of high-PRF exposures, such as bubble shielding or non-dissolution of bubbles between pulses. (Wang et al. 2012b). Pre-focal cavitation bubbles may prevent the acoustic energy from reaching the focus, as observed in other prior studies(Khokhlova et al. 2017b). High-speed photography showed the bubbles in the clouds occurring exclusively in the same location over all 2000 pulses, which could lead to liquefaction occurring only in those small areas, making it less effective. Additional experiments using high-PRF settings at extremely high pulse counts at almost half a million did show measurable damage in the lower stiffness 95/5 gel, but such a dose would be impractical to perform in clinical scenarios.

The trends observed with the pre vs post treatment elasticity for the hybrid gels and ex-vivo tissue demonstrate that the low-PRF exposure effectively liquifies them. No such significance was seen for any gel combination or the prostate with the high-PRF Low dose settings. At a higher dose however, the prostate and the weaker 95/5 gel showed a significant change in stiffness post treatment. For agarose phantoms, the use of indentometry was the only source of stiffness measurements aside from existing literature (Wilson et al. 2019). The indentometry technique could not measure the stiffness of the prostate samples due to their small dimensions. There was a consistent discrepancy between the shear wave and indentometry techniques measuring 24–33% lower for indentometry vs. SWE, which may be due to differences in the shear rates applied in each technique. Another limitation of the study was that the toughness of the hybrid gels and ex-vivo tissue samples were not directly measured. However, the toughness of similar hydrogels is reported in literature (Sun et al. 2012), and were further established through the dose response studies here.

This phantom may have multiple uses in the development of histotripsy therapies. For one, this gel could be expanded to test boiling histotripsy modalities, as preliminary experiments showed that these gels would not melt up near 100°C. The 3-dimensional nature and transparency of the gel also makes it easy to study the boiling bubble behavior under different exposures and provide further insights. We envision our future experiments to expand on this initial study to perform more systematic comparisons of histotripsy pulsing parameters, or complex treatment methodologies (Maxwell et al. 2014),(Duryea et al. 2014) to reduce treatment time while maintaining efficacy.

CONCLUSION:

This work demonstrated the formulation and use of a tough hydrogel from alginate-acrylamide that is optically transparent was found to mimic ex-vivo pathologic BPH tissue acoustic and mechanical properties. The phantoms had a response to histotripsy that could be measured by B-Mode ultrasound and SWE. The results further established that the hybrid hydrogels demonstrate similar lesion formation to ex-vivo human BPH tissue and can effectively be used to provide initial comparison of treatment parameters, providing immediate feedback. Such phantoms may be used precursory to translational studies to rapidly test the efficacy of different histotripsy parameters in treating BPH and other fibrous tissues.

Acknowledgements

We thank Ga Won Kim from the Center for Industrial and Medical Ultrasound for her help with collecting high speed camera data. We also acknowledge financial support from National Institutes of Health through R01-DK119310 and L30-DK122509.

REFERENCES:

Ambrogio S, Baêsso R de M, Gomis A, Rivens I, Gter Haar, Zeqiri B, Ramnarine KV, Fedele F, Miloro P. A Polyvinyl Alcohol-Based Thermochromic Material for Ultrasound Therapy Phantoms. Ultrasound Med Biol Elsevier, 2020;46:3135–3144.

Ambrogio S, Baêsso RM, Bosio F, Fedele F, Ramnarine KV, Zeqiri B, Miloro P. A standard test phantom for the performance assessment of magnetic resonance guided high intensity focused

ultrasound (MRgHIFU) thermal therapy devices. Int J Hyperth Taylor & Francis, 2022;39:57–68. Available from: 10.1080/02656736.2021.2017023

Bercoff J, Criton A, Bacrie CC, Souquet J, Tanter M, Gennisson JL, Deffieux T, Fink M, Juhan V, Colavolpe A, Amy D, Athanasiou A. ShearWaveTM elastography: A new real time imaging mode for assessing quantitatively soft tissue viscoelasticity. Proc - IEEE Ultrason Symp 2008;321–324.

Bt Ibrahim SF, Mohd Azam NAN, Amin KAM. Sodium alginate film: The effect of crosslinker on physical and mechanical properties. IOP Conf Ser Mater Sci Eng Institute of Physics Publishing, 2019;509.

Bush NL, Hill CR. Gelatine-alginate complex gel: A new acoustically tissue-equivalent material. Ultrasound Med Biol 1983;9.

Cabrelli LC, Grillo FW, Sampaio DRT, Carneiro AAO, Pavan TZ. Acoustic and Elastic Properties of Glycerol in Oil-Based Gel Phantoms. Ultrasound Med Biol 2017;43:2086–2094. [PubMed: 28648918]

Choi I, Shield RT. Second-order effects in problems for a class of elastic materials. Zeitschrift für Angew Math und Phys ZAMP 1981 324 Springer, 1981 [cited 2022 Mar 9];32:361–381. Available from: https://link.springer.com/article/10.1007/BF00955616

Choi MJ, Guntur SR, Lee KIL, Paeng DG, Coleman A. A Tissue Mimicking Polyacrylamide Hydrogel Phantom for Visualizing Thermal Lesions Generated by High Intensity Focused Ultrasound. Ultrasound Med Biol 2013;39:439–448. [PubMed: 23312531]

Clarke AJ, Evans JA, Truscott JG, Milner R, Smith MA. A phantom for quantitative ultrasound of trabecular bone. Phys Med Biol 1994;39.

Culjat MO, Goldenberg D, Tewari P, Singh RS. A review of tissue substitutes for ultrasound imaging. Ultrasound Med Biol 2010;36:861–873. [PubMed: 20510184]

Discher DE, Mooney DJ, Zandstra PW. Growth factors, matrices, and forces combine and control stem cells. Science NIH Public Access, 2009 [cited 2021 Oct 14];324:1673. Available from: /pmc/articles/PMC2847855/

Dunmire B, Kucewicz JC, Mitchell SB, Crum LA, Sekins KM. Characterizing an Agar/Gelatin phantom for image guided dosing and feedback control of high-intensity focused ultrasound. Ultrasound Med Biol 2013;39:300–311. [PubMed: 23245823]

Duryea A, Cain C, Tamaddoni H, Roberts W, Hall T. Removal of residual nuclei following a cavitation event using low-amplitude ultrasound. IEEE Trans Ultrason Ferroelectr Freq Control 2014;61:1619–1626. [PubMed: 25265172]

Eranki A, Mikhail AS, Negussie AH, Katti PS, Wood BJ, Partanen A. Tissue-mimicking thermochromic phantom for characterization of HIFU devices and applications. Int J Hyperthermia NIH Public Access, 2019 [cited 2022 Mar 17];36:518. Available from: /pmc/articles/PMC6625350/

Geoghegan R, Santamaria A, Priester A, Zhang L, Wu H, Grundfest W, Marks L, Natarajan S. A Tissue-Mimicking Prostate Phantom for 980nm Laser Interstitial Thermal Therapy. Int J Hyperthermia NIH Public Access, 2019 [cited 2021 Oct 21];36:993. Available from: /pmc/articles/PMC6827870/

Gong JP, Katsuyama Y, Kurokawa T, Osada Y. Double-network hydrogels with extremely high mechanical strength. Adv Mater 2003;15:1155–1158.

Guan Y, Lu M, Li Y, Liu F, Gao Y, Dong T, Wan M. Histotripsy Produced by Hundred-Microsecond-Long Focused Ultrasonic Pulses: A Preliminary Study. Ultrasound Med Biol 2016;42:2232–2244. [PubMed: 27318864]

Guntur SR, Choi MJ. An Improved Tissue-Mimicking Polyacrylamide Hydrogel Phantom for Visualizing Thermal Lesions with High-Intensity Focused Ultrasound. Ultrasound Med Biol 2014;40:2680–2691. [PubMed: 25220272]

Hall TL, Hempel CR, Wojno K, Xu Z, Cain CA, Roberts WW. Histotripsy of the Prostate: Dose Effects in a Chronic Canine Model. Urology Elsevier Inc., 2009;74:932–937. Available from: 10.1016/j.urology.2009.03.049

Hempel CR, Hall TL, Cain CA, Fowlkes JB, Xu Z, Roberts WW. Histotripsy fractionation of prostate tissue: Local effects and systemic response in a canine model. J Urol 2011;185.

Hendricks-Wenger A, Weber P, Simon A, Saunier S, Coutermarsh-Ott S, Grider D, Vidal-Jove J, Allen IC, Luyimbazi D, Vlaisavljevich E. Histotripsy for the Treatment of Cholangiocarcinoma Liver Tumors: In Vivo Feasibility and Ex Vivo Dosimetry Study. IEEE Trans Ultrason Ferroelectr Freq Control NLM (Medline), 2021;68:2953–2964.

Hori RY, Lewis JL. Mechanical properties of the fibrous tissue found at the bone-cement interface following total joint replacement. J Biomed Mater Res 1982;16:911–927. [PubMed: 7174716]

Ishigooka M, Hayami S, Hashimoto T, Suzuki Y, Katoh T, Nakada T. Relative and total volume of histological components in benign prostatic hyperplasia: Relationships between histological components and clinical findings. Prostate 1996;29.

Kharine A, Manohar S, Seeton R, Kolkman RGM, Bolt RA, Steenbergen W, de Mul FFM. Poly(vinyl alcohol) gels for use as tissue phantoms in photoacoustic mammography. Phys Med Biol 2003;48:357–370. [PubMed: 12608612]

Khokhlova TD, Haider YA, Maxwell AD, Kreider W, Bailey MR, Khokhlova VA. Dependence of Boiling Histotripsy Treatment Efficiency on HIFU Frequency and Focal Pressure Levels. Ultrasound Med Biol Elsevier USA, 2017a;43:1975–1985.

Khokhlova TD, Haider YA, Maxwell AD, Kreider W, Bailey MR, Khokhlova VA. Dependence of Boiling Histotripsy Treatment Efficiency on HIFU Frequency and Focal Pressure Levels. Ultrasound Med Biol 2017b;43:1975–1985. [PubMed: 28641910]

Khokhlova TD, Kucewicz JC, Ponomarchuk EM, Hunter C, Bruce M, Khokhlova VA, Matula TJ, Monsky W. Effect of Stiffness of Large Extravascular Hematomas on Their Susceptibility to Boiling Histotripsy Liquefaction in Vitro. Ultrasound Med Biol 2020;46:2007–2016. [PubMed: 32444137]

Kondo T, Kitatuji M, Shikinami Y, Tuta K, Kanda H. New tissue mimicking materials for ultrasound phantoms. Proc - IEEE Ultrason Symp IEEE, 2005;3:1664–1667.

Lin KW, Hall T, McGough R, Xu Z, Cain C. Synthesis of monopolar ultrasound pulses for therapy: The frequency-compounding transducer. IEEE Trans Ultrason Ferroelectr Freq Control IEEE, 2014a;61:1123–1136.

Lin KW, Kim Y, Maxwell A, Wang TY, Hall T, Xu Z, Fowlkes J, Cain C. Histotripsy beyond the intrinsic cavitation threshold using very short ultrasound pulses: Microtripsy. IEEE Trans Ultrason Ferroelectr Freq Control IEEE, 2014b;61:251–265.

Madsen EL, Frank GR, Dong F. Liquid or solid ultrasonically tissue-mimicking materials with very low scatter. Ultrasound Med Biol 1998;24:535–542. [PubMed: 9651963]

Mancia L, Vlaisavljevich E, Xu Z, Johnsen E. Predicting Tissue Susceptibility to Mechanical Cavitation Damage in Therapeutic Ultrasound. Ultrasound Med Biol Elsevier USA, 2017;43:1421–1440.

Mancia L, Vlaisavljevich E, Yousefi N, Rodriguez M, Ziemlewicz TJ, Lee FT, Henann D, Franck C, Xu Z, Johnsen E. Modeling tissue-selective cavitation damage. Phys Med Biol Institute of Physics Publishing, 2019;64.

Maxwell AD, Hsi RS, Bailey MR, Casale P, Lendvay TS. Noninvasive ureterocele puncture using pulsed focused ultrasound: An in vitro study. J Endourol 2014;28:342–346. [PubMed: 24171441]

Maxwell AD, Wang T-Y, Cain CA, Fowlkes JB, Sapozhnikov OA, Bailey MR, Xu Z. Cavitation clouds created by shock scattering from bubbles during histotripsy. J Acoust Soc Am 2011a;130:1888–1898. [PubMed: 21973343]

Maxwell AD, Wang T, Yuan L, Duryea AP, Xu Z, Cain CA. tissue phantom for measurement of US induced cavitation damage. 2011b;36:2132–2143.

Maxwell AD, Wang TY, Yuan L, Duryea AP, Xu Z, Cain CA. A tissue phantom for visualization and measurement of ultrasound-induced cavitation damage. Ultrasound Med Biol 2010a;36.

Maxwell AD, Wang TY, Yuan L, Duryea AP, Xu Z, Cain CA. A tissue phantom for visualization and measurement of ultrasound-induced cavitation damage. Ultrasound Med Biol 2010b;36:2132–2143. [PubMed: 21030142]

McDonald M, Lochhead S, Chopra R, Bronskill MJ. Multi-modality tissue-mimicking phantom for thermal therapy. Phys Med Biol Phys Med Biol, 2004 [cited 2022 Mar 17];49:2767–2778. Available from: https://pubmed.ncbi.nlm.nih.gov/15285246/ [PubMed: 15285246]

Morchi L, Gini M, Mariani A, Pagliarani N, Cafarelli A, Tognarelli S, Menciassi A. A Reusable Thermochromic Phantom for Testing High Intensity Focused Ultrasound Technologies. Proc Annu Int Conf IEEE Eng Med Biol Soc EMBS IEEE, 2021;1431–1434.

Moreland RB, Nehra A. Pathophysiology of Peyronie's disease. Int. J. Impot. Res. 2002.

Pogue BW, Patterson MS. Review of tissue simulating phantoms for optical spectroscopy, imaging and dosimetry. J Biomed Opt 2006;11:041102. [PubMed: 16965130]

Roberts WW, Hall TL, Ives K, Wolf JS, Fowlkes JB, Cain CA. Pulsed cavitational ultrasound: A noninvasive technology for controlled tissue ablation (histotripsy) in the rabbit kidney. J Urol 2006;175.

Roberts WW, Teofilovic D, Jahnke RC, Patri J, Risdahl JM, Bertolina JA. Histotripsy of the prostate using a commercial system in a canine model. J Urol Elsevier Ltd, 2014a;191:860–865. Available from: 10.1016/j.juro.2013.08.077

Roberts WW, Teofilovic D, Jahnke RC, Patri J, Risdahl JM, Bertolina JA. Histotripsy of the prostate using a commercial system in a canine model. J Urol 2014b;191:860–865. [PubMed: 24012583]

Rodriguez-Nieves JA, Macoska JA. Prostatic fibrosis, lower urinary tract symptoms, and BPH. Nat Rev Urol NIH Public Access, 2013 [cited 2021 Oct 1];10:546. Available from: /pmc/articles/PMC5625295/

Schade GR, Hall TL, Roberts WW. Urethral-sparing histotripsy of the prostate in a canine model. Urology Elsevier Inc, 2012;80:730–735. Available from: 10.1016/j.urology.2012.05.027

Schade GR, Styn NR, Ives KA, Hall TL, Roberts WW. Prostate histotripsy: Evaluation of prostatic urethral treatment parameters in a canine model. BJU Int 2014;113:498–503. [PubMed: 24176120]

Schuppan D, Afdhal NH. Liver cirrhosis. Lancet 2008;371:838–851. [PubMed: 18328931]

Schuster TG, Wei JT, Hendlin K, Jahnke R, Roberts WW. Histotripsy Treatment of Benign Prostatic Enlargement Using the Vortx Rx System: Initial Human Safety and Efficacy Outcomes. Urology Elsevier Inc, 2018;114:184–187. Available from: 10.1016/j.urology.2017.12.033

Shapiro E, Becich MJ, Hartanto V, Lepor H. The relative proportion of stromal and epithelial hyperplasia is related to the development of symptomatic benign prostate hyperplasia. J Urol 1992;147.

Stewart EA, Laughlin-Tommaso SK, Catherino WH, Lalitkumar S, Gupta D, Vollenhoven B. Uterine fibroids. Nat Rev Dis Prim 2016;2.

Sun JY, Zhao X, Illeperuma WRK, Chaudhuri O, Oh KH, Mooney DJ, Vlassak JJ, Suo Z. Highly stretchable and tough hydrogels. Nature Nature Publishing Group, 2012;489:133–136. Available from: 10.1038/nature11409

Szabo TL. Diagnostic Ultrasound Imaging: Inside Out: Second Edition. Diagnostic Ultrasound Imaging Insid Out Second Ed Elsevier Inc., 2004;1–549.

Tatarinov A, Pontaga I, Vilks U. Modeling the influence of mineral content and porosity on ultrasound parameters in bone by using synthetic phantoms. Mech Compos Mater 1999;35:147–154. Available from: 10.1007/BF02257245

Vlaisavljevich E, Gerhardson T, Hall T, Xu Z. Effects of f-number on the histotripsy intrinsic threshold and cavitation bubble cloud behavior. Phys Med Biol IOP Publishing, 2017;62:1269–1290.

Vlaisavljevich E, Kim Y, Owens G, Roberts W, Cain C, Xu Z. Effects of tissue mechanical properties on susceptibility to histotripsy-induced tissue damage. Phys Med Biol Institute of Physics Publishing, 2014;59:253–270.

Vlaisavljevich E, Lin KW, Warnez MT, Singh R, Mancia L, Putnam AJ, Johnsen E, Cain C, Xu Z. Effects of tissue stiffness, ultrasound frequency, and pressure on histotripsy-induced cavitation bubble behavior. Phys Med Biol Institute of Physics Publishing, 2015;60:2271–2292.

Wang TY, Hall TL, Xu Z, Fowlkes JB, Cain CA. Imaging feedback of histotripsy treatments using ultrasound transient elastography. IEEE Int Ultrason Symp IUS 2011;2233–2236.

Wang TY, Hall TL, Xu Z, Fowlkes JB, Cain CA. Imaging feedback of histotripsy treatments using ultrasound shear wave elastography. IEEE Trans Ultrason Ferroelectr Freq Control 2012a;59:1167–1181. [PubMed: 22711412]

Wang TY, Xu Z, Hall TL, Fowlkes JB, Cain CA. An Efficient Treatment Strategy for Histotripsy by Removing Cavitation Memory. Ultrasound Med Biol 2012b;38:753–766. [PubMed: 22402025]

Wang Y-N, Khokhova TD, Buravkov S, Chernikov V, Kreider W, Partanen A, Farr N, Maxwell A, Schade GR, Khokhlova VA. MECHANICAL DECELLULARIZATION OF TISSUE VOLUMES USING BOILING HISTOTRIPSY. Phys Med Biol NIH Public Access, 2018 [cited 2021 Oct 7];63:235023. Available from: /pmc/articles/PMC6527100/

Wells RG. Tissue Mechanics and Fibrosis. Biochim Biophys Acta NIH Public Access, 2013 [cited 2021 Oct 19];1832:884. Available from: /pmc/articles/PMC3641165/

Wilson CT, Hall TL, Johnsen E, Mancia L, Rodriguez M, Lundt JE, Colonius T, Henann DL, Franck C, Xu Z, Sukovich JR. Comparative study of the dynamics of laser and acoustically generated bubbles in viscoelastic media. Phys Rev E 2019;99.

Worthington AE, Trachtenberg J, Sherar MD. Ultrasound properties of human prostate tissue during heating. Ultrasound Med Biol 2002;28:1311–1318. [PubMed: 12467858]

Yamanaka T, Harimoto N, Hoshino K, Muranushi R, Hagiwara K, Gantumur D, Ishii N, Tsukagoshi M, Igarashi T, Watanabe A, Kubo N, Araki K, Shirabe K. Boiling histotripsy-induced mechanical ablation modulates tumour microenvironment by promoting immunogenic cell death of cancers. Ann Oncol Elsevier, 2019 [cited 2021 Dec 28];30:v20–v21. Available from: http://www.annalsofoncology.org/article/S0923753419583077/fulltext

Yang CH, Wang MX, Haider H, Yang JH, Sun JY, Chen YM, Zhou J, Suo Z. Strengthening alginate/polyacrylamide hydrogels using various multivalent cations. ACS Appl Mater Interfaces 2013;5:10418–10422. [PubMed: 24128011]

Yang S, Chen YJ, Cui R, Zhao HX, Zhao Y, Liu ZQ, Yu Y, Shao XY, Xu Q. High-intensity focused ultrasound ablation: An in vitro agarose gel model. Int J Clin Exp Med 2017;10:15302–15308.

Zell K, Sperl JI, Vogel MW, Niessner R, Haisch C. Acoustical properties of selected tissue phantom materials for ultrasound imaging. Phys Med Biol 2007;52.

Zhang J, Zhang M, Tang J, Yin G, Long Z, Leye He •, Zhou Chuanchi, Luo Lufeng, Qi L, Wang Long. Animal models of benign prostatic hyperplasia. Prostate Cancer Prostatic Dis 2021 [cited 2021 Oct 7];24:49–57. Available from: 10.1038/s41391-020-00277-1 [PubMed: 32873917]

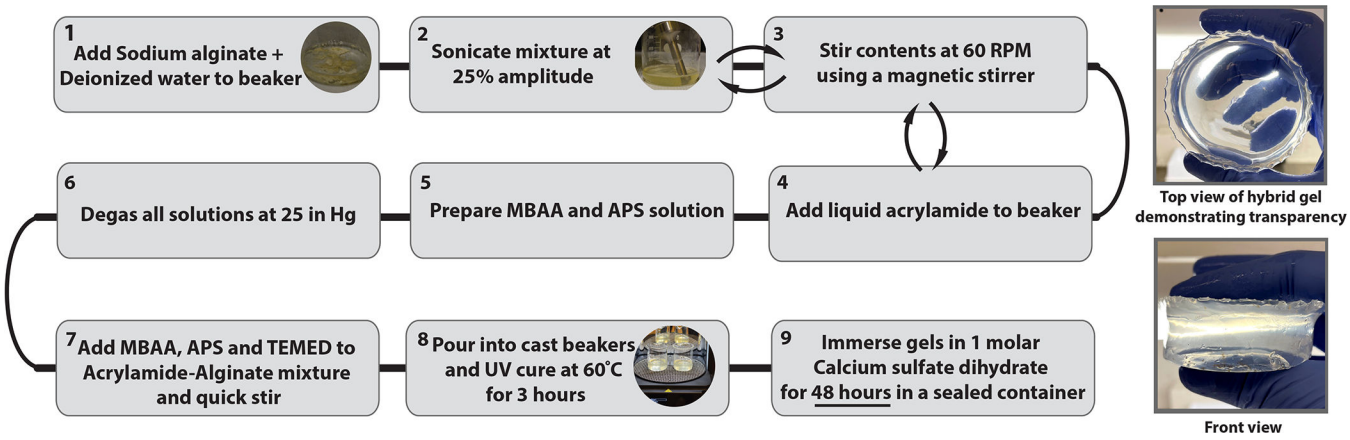

Figure 1:

Flowchart summarizing the preparation for Polyacrylamide/Alginate hybrid gel phantoms. The righthand images show the appearance of the final hydrogel, which has high optical transparency.

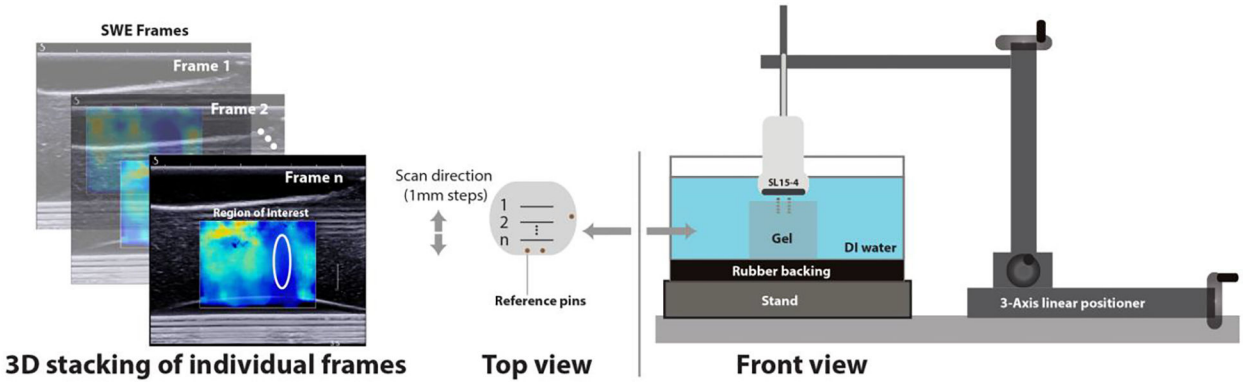

Figure 2:

Experimental setup demonstrating the method for acquiring a 3-dimensional SWE map of hybrid gels. (Right) A SL15–4 imager is held above the gel in a water bath in cross-sections aligned by reference pins. (Left) Individual B-mode and SWE frames were acquired for each cross section to estimate uniformity and stiffness.

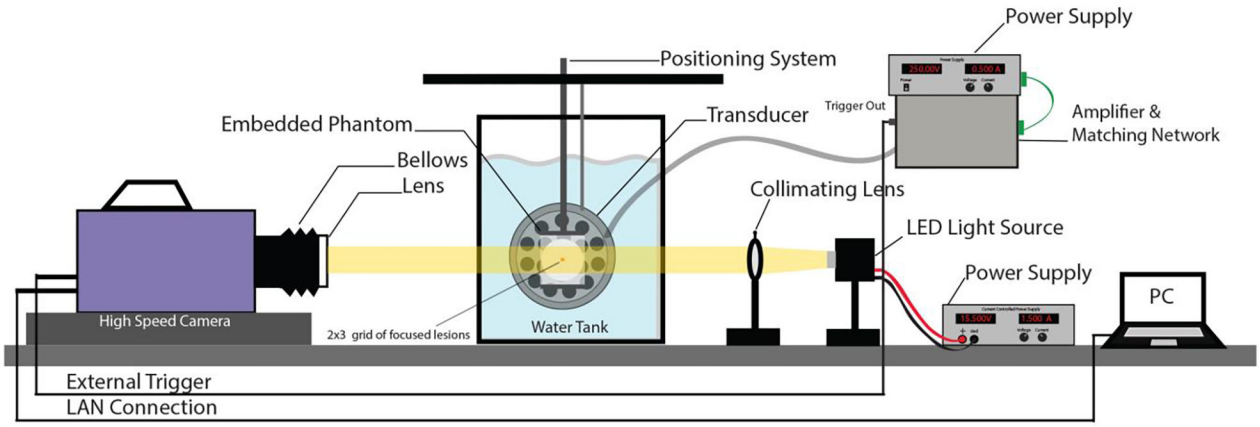

Figure 3:

High speed camera setup for bench top bubble visualization experiments. An LED source is used for back illumination through the gel. The transducer is aligned orthogonally to the camera and focused into the gel in the field of view. An external PC is used to record the captured images from the camera.

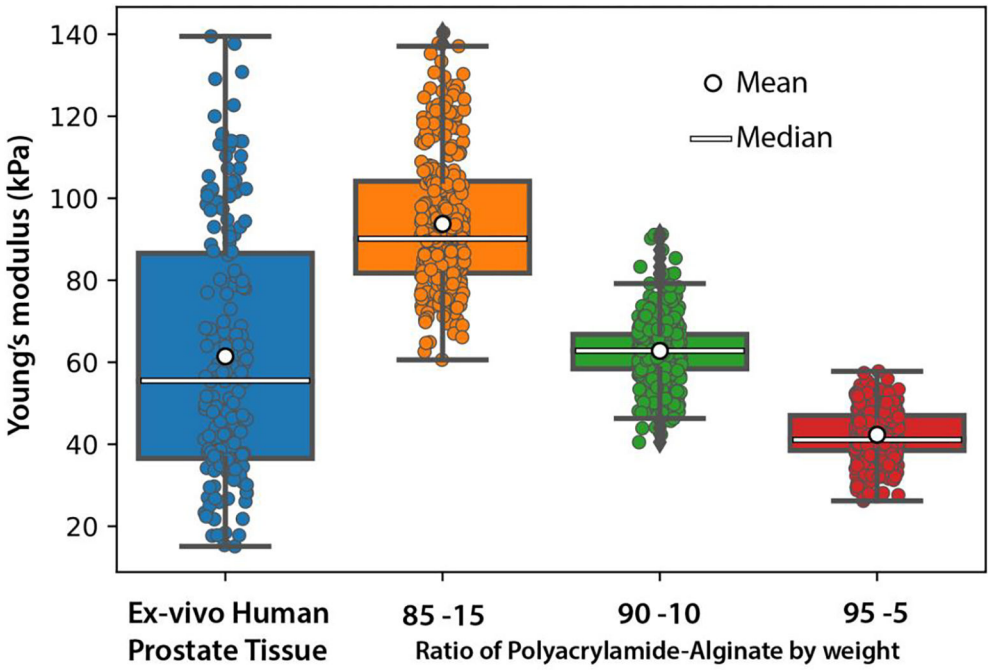

Figure 4:

Measured Young's moduli for different compositions of polyacrylamide/alginate hybrid gels and ex-vivo human prostate tissue. Varying the ratio of acrylamide to alginate allows approximation of ex-vivo human prostate tissue across its stiffness range.

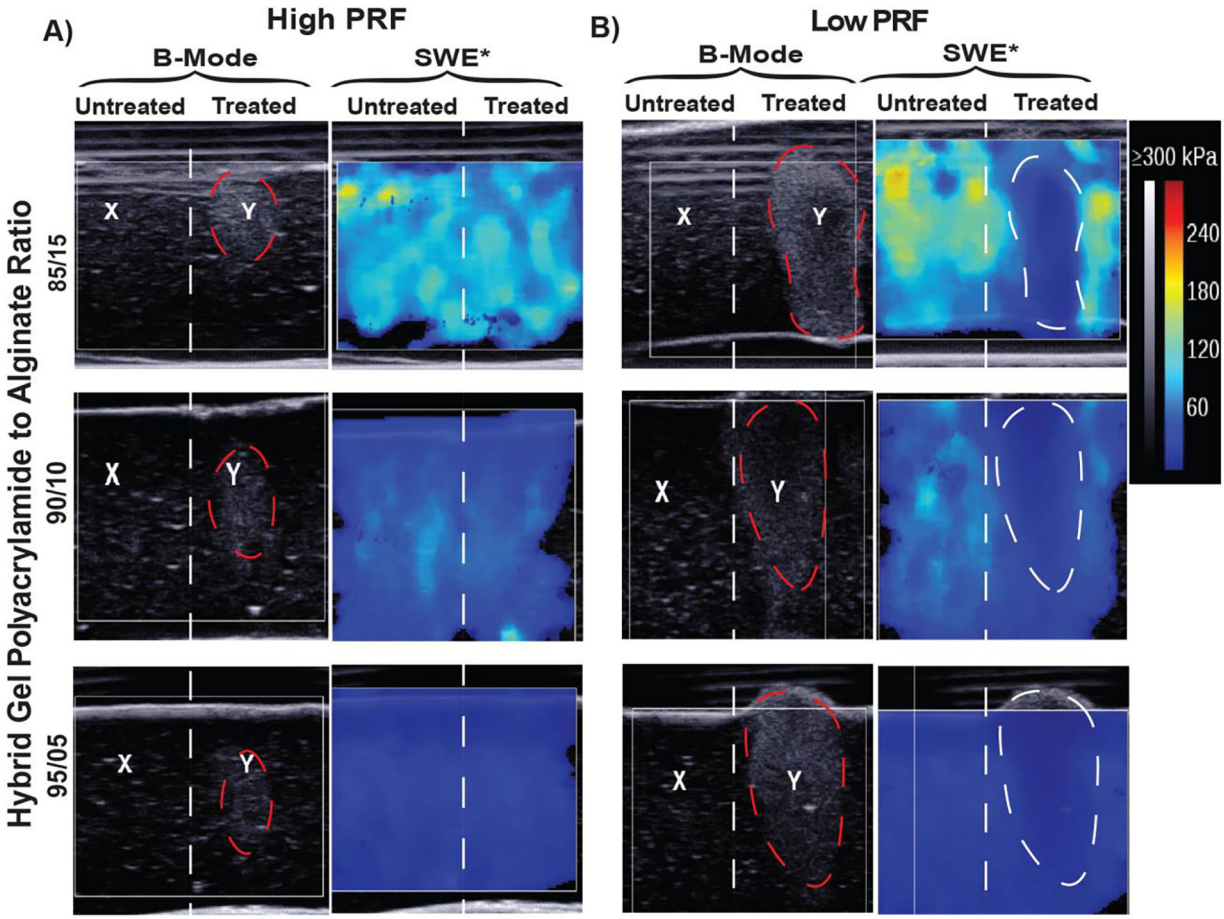

Figure 5:

Evaluation of histotripsy induced damage in acrylamide/alginate hybrid gels with B-mode and shear wave elastography (SWE) A) B-mode and SWE evaluation of high-PRF parameter settings showing hyperechoic bubble formation on B-mode (highlighted in red) and failure of treatment to induce changes in SWE color map B) B-mode and SWE evaluation of low-PRF parameter settings showing hypo + hyperechoic changes on B-mode (highlighted in red) and corresponding distinct changes in the SWE color map (highlighter in white). The X on B-mode indicated an untreated region while the Y denotes treated region.

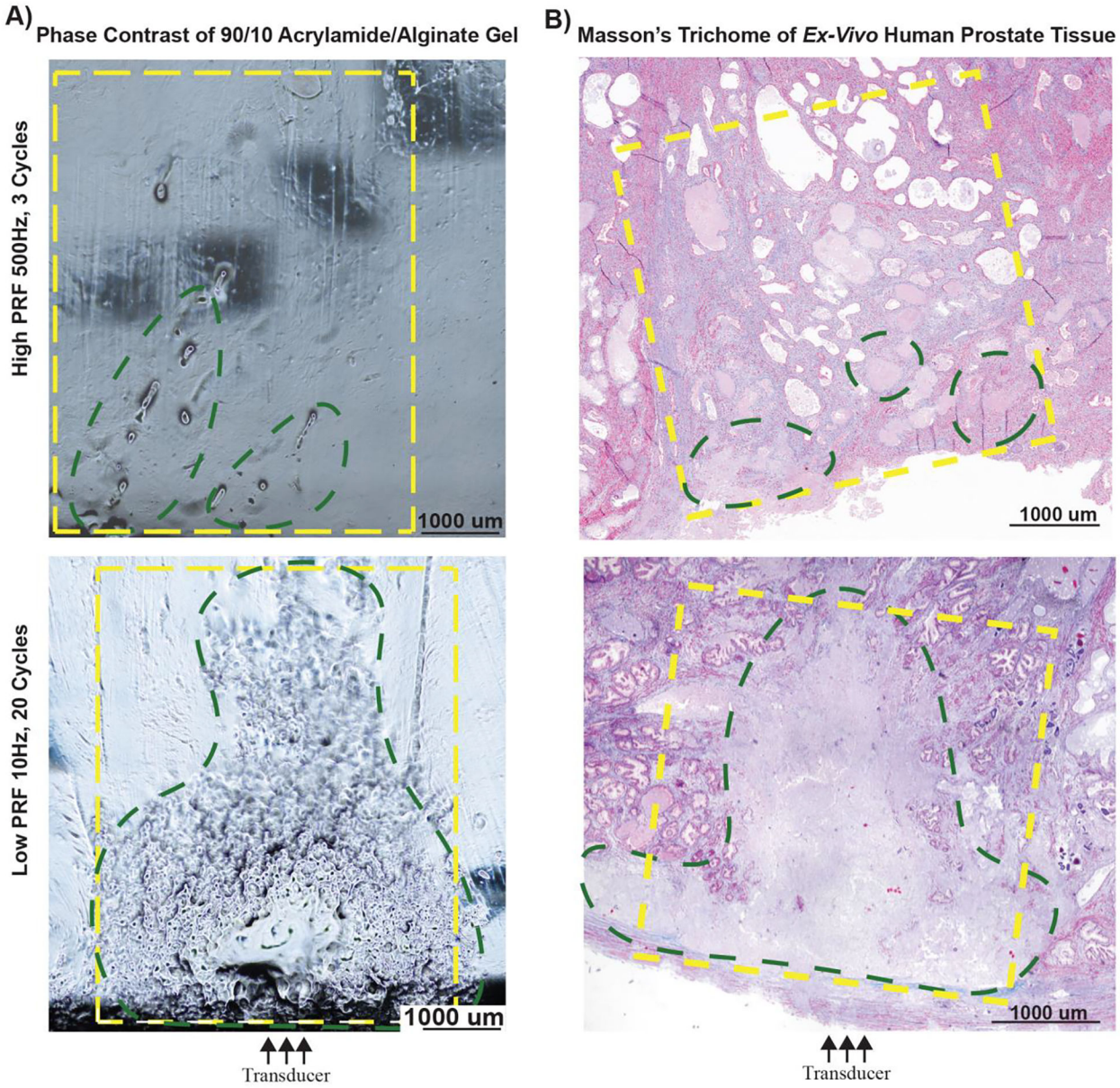

Figure 6:

Correlating treatment effects in polyacrylamide/alginate gels to lesion formation in ex-vivo human prostate tissue; green outline indicated areas of histotripsy damage and yellow outline denotes area of intended/expected treatment A) Evaluation of histotripsy induced damage under phase contrast microscopy in hybrid gels between treatment area (green) and expected treatment area (yellow). B) Masson's trichrome stained ex-vivo human prostate tissue, showing a complete homogenized lesion (green) within the expected treatment area (yellow).

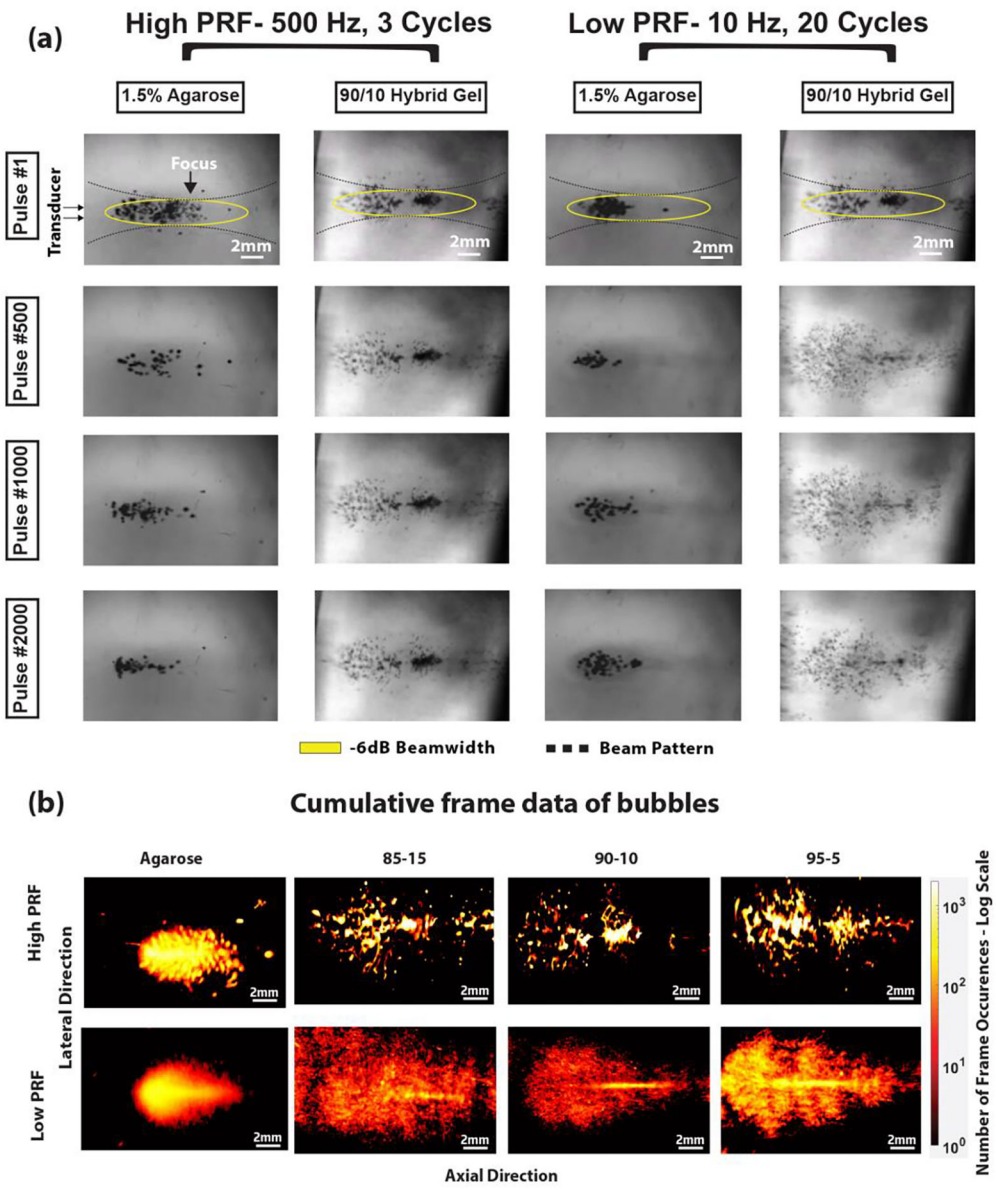

Figure 7:

(A) High speed camera images showing cavitation cloud progression in agarose vs acrylamide/alginate hybrid gels at both high-PRF and low-PRF parameters. (B) Superimposed bubble clouds from all 2000 frames, with the dynamic range of frames measured varying across Low and high-PRF settings, with the white arrows encompassing the total cumulative cloud observed.

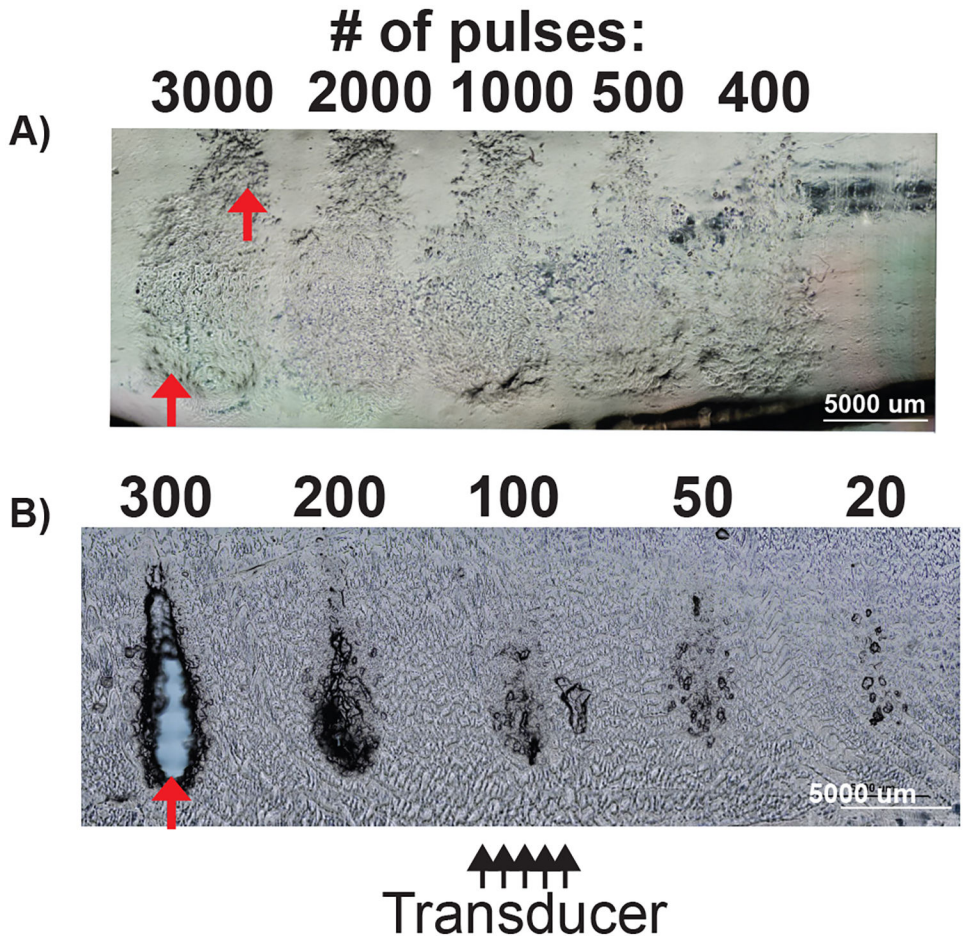

Figure 8:

Phase contrast image for low-PRF parameter settings in 85/15 polyacrylamide gel vs 1.5% agarose gel A) 85/15 polyacrylamide gel showing progressive refractive changes indicating damage at increasing pulse count. The cavity present is denoted by red arrows (B) Dose response evaluation in 1.5% agarose gel showing cavity formation that progresses to a portion of the beamwidth at 200 pulses with complete cavity formation (fully defined lesion) at 300 pulses (red arrow).

Table 1.

Sample weight and volume measurements for preparing 200 g of 85:15 Polyacrylamide Alginate gel.

Chemical Name	Wt% from recipe	Final Quantities
Deionized Water	86%	107.03 mL
Acrylamide	11.9%	59.5 mL
Alginate	2.1%	4.2 g
Sum Total	**100%**	
AP	0.17% of Acrylamide	From 1% AP - 4.046 mL
MBAA	0.06% of Acrylamide	From 1% MBAA - 1.428 mL
TEMED	0.28% of Acrylamide	0.052 mL

1M solution of $CaSO_4.2H_2O$ is prepared by mixing 136.14 g in 1 liter of deionized water

Table 2.

Treatment Paradigms

Parameters	Frequency (kHz)	Pulse Repetition Frequency (Hz)	Pulse Duration (cycles)	Mean Peak Positive Pressure (MPa)*	Mean Peak Negative Pressure (MPa)*
high-PRF	700	500	3	54–108	14–20
low-PRF	700	10	20	95–108	16.6–20

* For dose response, volumetric treatment, and prostate tissue experiments

Table 3.

Mean and percent deviation of the Youngs's modulus of the hybrid gels and tissue as measured using SWE.

Gel Type	Mean ± St. Dev. (kPa)	% Deviation
85/15	93.73±16.67	17.78
90/10	62.77±7.28	11.6
95/5	42.33±6.011	14.2
EVHP	61.44±29.77	48.45

Table 4.

Indentometry vs Shear Wave of Hybrid Gels

Gel Type	Indentometry Measured Range (kPa)	SWE Measured Range (kPa)	% Difference from SWE
85/15	48.25±12.06	63.62±21.51	24.15
90/10	25.41±3.97	37.51±8.56	32.25
95/5	7.87±8.80	11.72±0.10	32.81

Table 5.

Acoustic properties of polyacrylamide/alginate hybrid gels in comparison to agarose gels and prostate

Gel Type	Attenuation (dB/cm/MHz)	Speed of Sound (m/s)	Density (Kg/m3)	Impedance (MRayls)
85/15	−0.06 ± 0.01	1528 ±6	1024 ±18	1.57 ±.03
90/10	−0.07 ± 0.04	1514 ±5	1020 ±13	1.54 ±.03
95/05	−0.14± 0.06	1520 ±5	1056 ±24	1.61 ±.04
*__Agarose__ [1]	−0.04 – −0.46 dB/cm	1503 – 1526 m/s		
*__Prostate__ [2]	−0.72 dB/cm/MHz	1530 m/s		

*Values derived from literature

[1](Yang et al. 2017)

[2](Worthington et al. 2002)

Table 6.

Response of the hybrid gels and the tissue to different histotripsy parameters

Treatment Setting	Medium	Elasticity change (posttreatment – pretreatment, kPa)	P Value
high-PRF – Low Dose	85/15	−13.5	0.129
	90/10	−6.5	0.496
	95/05	−22.5	<0.005 *
	Prostate	−15.5	0.0742
high-PRF – High Dose	85/15	1.5	0.910
	90/10	−5.5	0.5703
	95/05	−22.5	<0.005 *
	Prostate	−26.0	<0.05 *
low-PRF	85/15	−20.5	<0.005 *
	90/10	−22.5	<0.005 *
	95/05	−22.5	<0.005 *
	Prostate	−22.5	<0.005 *

* Statistically significant.